Available online at www.sciencedirect.com
ScienceDirect
International Journal of Multiphase Flow 33 (2007) 726–741
International Journal of Multiphase Flow
www.elsevier.com/locate/ijmulflow

Creeping motion of a slip spherical particle in a circular cylindrical pore

H.J. Keh *, Y.C. Chang

Department of Chemical Engineering, National Taiwan University, Taipei 10617, Taiwan, ROC

Received 19 July 2006; received in revised form 15 October 2006

Abstract

A combined analytical–numerical study for the creeping flow caused by a spherical fluid or solid particle with a slip-flow surface translating in a viscous fluid along the centerline of a circular cylindrical pore is presented. To solve the axisymmetric Stokes equations for the fluid velocity field, a general solution is constructed from the superposition of the fundamental solutions in both cylindrical and spherical coordinate systems. The boundary conditions are enforced first at the pore wall by the Fourier transforms and then on the particle surface by a collocation technique. Numerical results for the hydrodynamic drag force acting on the particle are obtained with good convergence for various values of the relative viscosity or slip coefficient of the particle, the slip parameter of the pore wall, and the ratio of radii of the particle and pore. For the motion of a fluid sphere along the axis of a cylindrical pore, our drag results are in good agreement with the available solutions in the literature. As expected, the boundary-corrected drag force for all cases is a monotonic increasing function of the ratio of particle-to-pore radii, and approaches infinity in the limit. Except for the case that the cylindrical pore is hardly slip and the value of the ratio of particle-to-pore radii is close to unity, the drag force exerted on the particle increases monotonically with an increase in its relative viscosity or with a decrease in its slip coefficient for a constant ratio of radii. In a comparison for the pore shape effect on the axial translation of a slip sphere, it is found that the particle in a circular cylindrical pore in general acquires a lower hydrodynamic drag than in a spherical cavity, but this trend can be reversed for the case of highly slippery particles and pore walls.

Keywords: Creeping flow; Fluid droplet; Aerosol sphere; Small pore; Slip-flow surface; Boundary effects

1. Introduction

The movement of a solid particle or fluid droplet through a continuous medium at low Reynolds numbers is of much interest in the fields of chemical, biomedical, and environmental engineering and science. The majority of these moving phenomena are fundamental in nature, but permit one to develop rational understanding of many practical systems and industrial processes such as sedimentation, flotation, coagulation, meteorology,

* Corresponding author. Tel.: +886 2 3366 3048; fax: +886 2 2362 3040.
E-mail address: huan@ntu.edu.tw (H.J. Keh).

0301-9322/$ - see front matter © 2007 Elsevier Ltd. All rights reserved.
doi:10.1016/j.ijmultiphaseflow.2006.12.008

suspension rheology, and motion of blood cells in an artery or vein. The theoretical study of this subject has grown out of the classic work of Stokes (1851) for a translating, no-slip, rigid sphere in an incompressible, Newtonian fluid.

The creeping-flow translation of a single spherical fluid drop of radius a in an unbounded medium of viscosity η was first analyzed independently by Hadamard (1911) and Rybczynski (1911). Assuming continuous velocity and continuous tangential stress across the interface between the fluid phases in the absence of surface active agents, they found that the drag force acting on the fluid sphere by the surrounding fluid is

$$\mathbf{F}_0 = -6\pi\eta a \frac{3\eta^* + 2}{3\eta^* + 3}\mathbf{U}, \tag{1}$$

where $\mathbf{U}$ is the drop velocity and η^* is the internal-to-external viscosity ratio. Since the fluid properties are arbitrary, Eq. (1) degenerates to the case of motion of a solid sphere (Stokes' law) when the viscosity of the drop becomes infinity and to the case of motion of a spherical gas bubble when the viscosity approaches zero.

In the general formulation of the Stokes problem, it is usually assumed that no slippage arises at the solid–fluid interfaces. Actually, this is an idealization of the transport processes involved. The phenomena that the adjacent fluid can slip frictionally over a solid surface, occurring for cases such as the low-density gas flow surrounding an aerosol particle (Kennard, 1938; Hutchins et al., 1995), the aqueous liquid flow near a hydrophobic surface (Tretheway and Meinhart, 2002; Gogte et al., 2005), and the Newtonian fluid flow over a porous surface (Beavers and Joseph, 1967; Saffman, 1971; Jones, 1973; Nir, 1976), have been confirmed, both experimentally and theoretically. Presumably, any such slipping would be proportional to the local tangential stress next to the solid surface (Happel and Brenner, 1983), known as the Navier slip (see Eqs. (19) and (20)), at least as long as the velocity gradient is small. The constant of proportionality, β^{-1}, is called a "slip coefficient". Basset (1961) found that the drag force exerted by the ambient fluid on a moving rigid sphere with a slip-flow boundary condition at its surface is

$$\mathbf{F}_0 = -6\pi\eta a \frac{\beta a + 2\eta}{\beta a + 3\eta}\mathbf{U}, \tag{2}$$

where $\mathbf{U}$ is the migration velocity of the particle. In the particular case of $\beta \to \infty$, there is no slip at the particle surface and Eq. (2) degenerates to Stokes' law. When $\beta = 0$, there is a perfect slip at the particle surface and Eq. (2) is identical to Eq. (1) taking $\eta^* = 0$. Note that, as can be seen from Eqs. (1) and (2), the unbounded flow field caused by the migration of a slip solid sphere is the same as the external flow field generated by the same motion of a spherical fluid drop with a value of η^* equal to the parameter $\beta a/3\eta$ of the solid sphere.

The slip coefficient in Eq. (2) has been determined experimentally for various gas–solid systems and found to agree with the general kinetic theory of gases. It can be calculated from the formula

$$\frac{\eta}{\beta} = C_m l, \tag{3}$$

where l is the mean free path of a gas molecule, and C_m is a dimensionless constant of the gas-kinetic slip, which is semi-empirically related to the momentum accommodation coefficient f_m at the solid surface by $C_m \approx (2 - f_m)/f_m$ (Kennard, 1938). Although C_m surely depends upon the nature of the surface and adjacent fluid, an examination of the experimental data and theoretical predictions suggests that it will be in the range 1.0–1.5 (Davis, 1972; Talbot et al., 1980; Sharipov and Kalempa, 2003). The quantity η/β is a length, which can be pictured by noting that the fluid motion is the same as if the solid surface is displaced inward by a distance η/β with the velocity gradient extending uniformly right up to no-slip velocity at the surface. The reciprocal of the factor $(\beta a + 2\eta)/(\beta a + 3\eta)$ in Eq. (2) is equivalent to the so-called Cunningham correction factor for the slip effect.

In real situations of the low-Reynolds-number motion, particles or droplets usually are not isolated and will move in the presence of neighboring boundaries. Using spherical bipolar coordinates, Bart (1968) and Rushton and Davies (1973) examined the motion of a spherical fluid drop settling normal to a plane interface between two immiscible viscous fluids. Wacholder and Weihs (1972) also utilized bipolar coordinates to study the motion of a fluid sphere through another fluid normal to a no-slip or free planar surface; their calculations agree with the results obtained by Bart in these limits. Recently, the slow motion of a fluid sphere perpendicular

to two parallel plane walls at an arbitrary position between them has been investigated with the use of a boundary collocation method (Chang and Keh, 2006). Numerical solutions for the hydrodynamic drag force acting on the droplet were obtained as functions of η^* and the respective relative distances from the droplet center to the two plane walls.

On the other hand, Haberman and Sayre (1958) considered a spherical fluid droplet in axisymmetric motion in a long tube filled with a viscous fluid and obtained a hydrodynamic drag solution using an approximate technique of matching the two series-expansion solutions in the spherical and cylindrical coordinate frames which is accurate only for about $a/b \leqslant 0.5$, where a and b are the radii of the droplet and tube, respectively. The wall effects experienced by a fluid sphere moving along the axis of a long tube were also examined by using a reciprocal theorem (Brenner, 1971) and a numerical least-square method correct for $a/b \leqslant 0.75$ (Coutanceau and Thizon, 1981). Hyman and Skalak (1972) used a singularity technique to perform numerical computations of the axisymmetric flow due to a train of equally spaced spherical droplets in a tube, considering the motion as a function of the relative droplet separation, a/b, and η^*, up to $a/b = 0.8$. Hetsroni et al. (1970) used a method of reflections to solve for the terminal velocity of a fluid sphere settling axially at an arbitrary radial location within a long tube. The parallel motion of a spherical droplet in a quiescent immiscible fluid at an arbitrary position between two parallel plane walls was also studied by Shapira and Haber (1988) using a method of reflections and by Keh and Chen (2001) using the boundary collocation technique.

The boundary effects on the motion of solid particles with finite values of $\beta a/\eta$ are different, both physically and mathematically, from those on fluid droplets of finite viscosities. Through an exact representation in spherical bipolar coordinates, Reed and Morrison (1974) and Chen and Keh (1995) examined the creeping motion of a rigid sphere normal to an infinite plane wall, where the fluid may slip at the solid surfaces. Later, the quasisteady translation of a slip spherical particle in a slip spherical cavity was also theoretically studied (Keh and Chang, 1998; Lu and Lee, 2001). An analytical expression for the wall-corrected drag force exerted by the fluid on the particle located at the center of the cavity was derived in a closed form. Recently, the slow translational and rotational motions of a slip sphere parallel (Chen and Keh, 2003) or perpendicular (Chang and Keh, 2006) to two parallel plane walls at an arbitrary position between them have been examined using the boundary collocation method. Numerical results for the hydrodynamic drag force and torque exerted on the particle were obtained as functions of $\beta a/\eta$ and the respective relative distances from the particle center to the two plane walls.

The objective of this work is to obtain exact solutions for the slow translational motion of a spherical fluid or solid particle along the centerline of a long circular cylindrical pore, where the fluid is allowed to slip at the particle and pore surfaces. The creeping-flow equations applicable to the systems are solved by using a combined analytical–numerical method with the boundary collocation technique (Leichtberg et al., 1976), and the wall-corrected drag force acting on the particle by the fluid is obtained with good convergence for various cases up to $a/b = 0.995$. Our calculations show very good agreement with the available solutions in the literature. Some comparisons for the pore shape effects on the axial translation of the slip particle are made.

2. Formulation for the motion of a fluid sphere along the axis of a circular cylindrical pore

In this section, we consider the steady creeping motion caused by a spherical fluid droplet of radius a translating with a velocity $\mathbf{U} = U\mathbf{e}_z$ in a second, immiscible fluid along the axis of a long circular cylindrical pore of radius b, where $b > a$, as shown in Fig. 1. Here (ρ, ϕ, z) and (r, θ, ϕ) denote the cylindrical and spherical coordinate systems, respectively, with the origin at the droplet center, and $\mathbf{e}_z$ is the unit vector in the z direction. The external fluid is at rest far away from the droplet. The purpose is to determine the correction to Eq. (1) for the motion of the droplet due to the presence of the pore wall.

Both of the fluids inside and outside the droplet are assumed to be incompressible and Newtonian. Owing to the low Reynolds numbers, the fluid motion is governed by the steady fourth-order differential equations for viscous axisymmetric creeping flows,

$$E^2(E^2\Psi) = 0 \quad (r \geqslant a), \tag{4a}$$

$$E^2(E^2\Psi_1) = 0 \quad (r \leqslant a), \tag{4b}$$

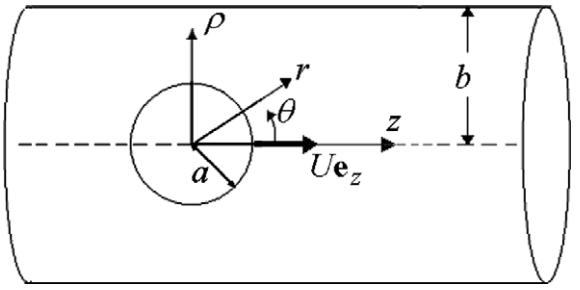

Fig. 1. Geometric sketch of the translation of a spherical particle along the axis of a circular cylindrical pore.

where Ψ_1 and Ψ are the Stokes stream functions for the flow inside the droplet and for the external flow, respectively, which are related to their corresponding velocity components in cylindrical coordinates by

$$v_\rho = \frac{1}{\rho}\frac{\partial \Psi}{\partial z}, \quad v_z = -\frac{1}{\rho}\frac{\partial \Psi}{\partial \rho}, \tag{5a}$$

$$v_{1\rho} = \frac{1}{\rho}\frac{\partial \Psi_1}{\partial z}, \quad v_{1z} = -\frac{1}{\rho}\frac{\partial \Psi_1}{\partial \rho}, \tag{5b}$$

and the Stokes operator E^2 has the form

$$E^2 = \rho\frac{\partial}{\partial \rho}\left(\frac{1}{\rho}\frac{\partial}{\partial \rho}\right) + \frac{\partial^2}{\partial z^2}. \tag{6}$$

The boundary conditions for the fluid flow field at the droplet surface, where both velocity and shear stress are continuous, on the pore wall, and far away from the droplet are

$$r = a: \qquad v_\rho = v_{1\rho}, \tag{7a}$$

$$v_z = v_{1z}, \tag{7b}$$

$$v_\rho \tan\theta + v_z = U, \tag{7c}$$

$$\tau_{r\theta} = \tau_{1r\theta}, \tag{7d}$$

$$\rho = b: \qquad v_\rho = v_z = 0, \tag{8}$$

$$|z| \to \infty: \qquad v_\rho = v_z = 0. \tag{9}$$

Here, $\tau_{r\theta}$ and $\tau_{1r\theta}$ are the viscous shear stresses for the external flow and the flow inside the droplet, respectively. The capillary number $\eta U/\gamma$ (and thus the smaller Weber number $a\rho_f U^2/\gamma$, where ρ_f is the density of the external fluid) is assumed to be sufficiently small (say, less than 0.1) so that the interfacial tension γ is fairly large to maintain the spherical shape of the droplet during the confined migration.

To solve the external flow field, we express the stream function, which is symmetric about the plane $z = 0$, in the form

$$\Psi = \Psi_w + \Psi_p. \tag{10}$$

Here Ψ_w is a separable solution of Eq. (4a) in cylindrical coordinates that represents the disturbance produced by the pore wall and is given by a Fourier–Bessel integral (Leichtberg et al., 1976),

$$\Psi_w = \int_0^\infty [X(\omega)\rho I_1(\omega\rho) + Y(\omega)\rho^2 I_0(\omega\rho)]\cos(\omega z)\,\mathrm{d}\omega, \tag{11}$$

where $X(\omega)$ and $Y(\omega)$ are unknown functions of the separation variable ω. The second part of Ψ, denoted by Ψ_p, is a separable solution of Eq. (4a) in spherical coordinates representing the disturbance generated by the droplet and is given by

$$\Psi_p = \sum_{n=2}^{\infty} (B_n r^{-n+1} + D_n r^{-n+3}) G_n^{-1/2}(\cos\theta) \quad (n \text{ is even}), \tag{12}$$

where $G_n^{-1/2}$ is the Gegenbauer polynomial of the first kind of order n and degree $-1/2$; B_n and D_n are unknown constants. Note that boundary condition (9) is immediately satisfied by a solution of the form given by Eqs. (10)–(12).

The general solution to Eq. (4b) for the internal flow field can be expressed as

$$\Psi_1 = \sum_{n=2}^{\infty} (A_n r^n + C_n r^{n+2}) G_n^{-1/2}(\cos\theta), \tag{13}$$

or

$$v_{1\rho} = \sum_{n=2}^{\infty} \left[A_n \alpha_{1n}^{(1)}(r,\theta) + C_n \alpha_{2n}^{(1)}(r,\theta) \right], \tag{14a}$$

$$v_{1z} = \sum_{n=2}^{\infty} \left[A_n \alpha_{1n}^{(2)}(r,\theta) + C_n \alpha_{2n}^{(2)}(r,\theta) \right] \quad (n \text{ is even}), \tag{14b}$$

where the definitions of the functions $\alpha_{in}^{(j)}(r,\theta)$ for i and j equal to 1 or 2 are given by Eqs. (A.1) and (A.2) in Appendix A, and A_n and C_n are unknown constants. A solution of this form satisfies the requirement that the velocity is finite for any position within the droplet.

Substituting the stream function Ψ given by Eqs. (10)–(12) into boundary condition Eq. (8) and applying the Fourier cosine transform on the variable z lead to a solution for the functions $X(\omega)$ and $Y(\omega)$ in terms of the coefficients B_n and D_n. After the substitution of this solution back into Eqs. (10)–(12) and utilization of Eq. (5a) and the integral representations of the modified Bessel functions, the external fluid velocity components can be expressed as

$$v_\rho = \sum_{n=2}^{\infty} \left[B_n \gamma_{1n}^{(1)}(r,\theta) + D_n \gamma_{2n}^{(1)}(r,\theta) \right], \tag{15a}$$

$$v_z = \sum_{n=2}^{\infty} \left[B_n \gamma_{1n}^{(2)}(r,\theta) + D_n \gamma_{2n}^{(2)}(r,\theta) \right], \tag{15b}$$

where n is even and the definitions of the functions $\gamma_{in}^{(j)}(r,\theta)$ for i and j equal to 1 or 2 are given by Eqs. (A.3) and (A.4) (in integral forms which must be evaluated numerically) taking $\beta_w \to \infty$.

The only boundary conditions that remain to be satisfied are those on the droplet surface. Substituting Eqs. (14) and (15) into Eq. (7), one obtains

$$\sum_{n=2}^{\infty} \left[B_n \gamma_{1n}^{(1)}(a,\theta) + D_n \gamma_{2n}^{(1)}(a,\theta) - A_n \alpha_{1n}^{(1)}(a,\theta) - C_n \alpha_{2n}^{(1)}(a,\theta) \right] = 0, \tag{16a}$$

$$\sum_{n=2}^{\infty} \left[B_n \gamma_{1n}^{(2)}(a,\theta) + D_n \gamma_{2n}^{(2)}(a,\theta) - A_n \alpha_{1n}^{(2)}(a,\theta) - C_n \alpha_{2n}^{(2)}(a,\theta) \right] = 0, \tag{16b}$$

$$\sum_{n=2}^{\infty} \left\{ B_n \left[\gamma_{1n}^{(1)}(a,\theta)\tan\theta + \gamma_{1n}^{(2)}(a,\theta) \right] + D_n \left[\gamma_{2n}^{(1)}(a,\theta)\tan\theta + \gamma_{2n}^{(2)}(a,\theta) \right] \right\} = U, \tag{16c}$$

$$\sum_{n=2}^{\infty} \left[B_n \gamma_{1n}^{*}(a,\theta) + D_n \gamma_{2n}^{*}(a,\theta) - \eta^* A_n \alpha_{1n}^{*}(a,\theta) - \eta^* C_n \alpha_{2n}^{*}(a,\theta) \right] = 0, \tag{16d}$$

where the functions $\alpha_{in}^{*}(r,\theta)$ and $\gamma_{in}^{*}(r,\theta)$ for $i = 1$ or 2 are defined by Eqs. (A.11) and (A.12) (in which the integration must be performed numerically) taking $\beta_w \to \infty$.

To satisfy the conditions in Eq. (16) exactly along the entire surface of the droplet would require the solution of the entire infinite array of unknown constants A_n, C_n, B_n, and D_n. However, the collocation method (O'Brien, 1968; Leichtberg et al., 1976) enforces the boundary conditions at a finite number of discrete points on the quarter-circular longitudinal arc of the sphere (from $\theta = 0$ to $\theta = \pi/2$, owing to the symmetry

of the system geometry) and truncates the infinite series in Eqs. (13)–(15) into finite ones. If the spherical boundary is approximated by satisfying the conditions in Eq. (7) at N discrete points on the generating arc, the infinite series in Eqs. (13)–(15) are truncated after N terms, resulting in a system of $4N$ simultaneous linear algebraic equations in the truncated form of Eq. (16). This matrix equation can be numerically solved to yield the $4N$ unknown constants A_n, C_n, B_n, and D_n required in the truncated form of Eqs. (14) and (15). The fluid velocity field is completely obtained once these coefficients are solved for a sufficiently large number of N. The accuracy of the boundary-collocation/truncation technique can be improved to any degree by taking a sufficiently large value of N. Naturally, as $N \to \infty$, the truncation error vanishes and the overall accuracy of the solution depends only on the numerical integration required in evaluating the functions $\gamma_{\text{in}}^{(j)}$ and γ_{in}^{*} in Eq. (16).

The drag force $\mathbf{F} = F\mathbf{e}_z$ exerted by the fluid on the droplet can be determined from (Happel and Brenner, 1983)

$$F = 4\pi\eta D_2. \tag{17}$$

This expression shows that only the lowest-order coefficient D_2 contributes to the hydrodynamic force acting on the droplet.

3. Solutions for the motion of a fluid sphere along the axis of a circular cylindrical pore

The numerical results for the creeping motion of a spherical fluid droplet of an arbitrary viscosity along the axis of a circular cylindrical pore, obtained by using the boundary collocation method described in the previous section, are presented in this section. The system of linear algebraic equations to be solved for the coefficients A_n, C_n, B_n, and D_n is constructed from Eq. (16). All the numerical integrations to evaluate the functions $\gamma_{\text{in}}^{(j)}$ and γ_{in}^{*} were done by using the method of Gauss-Laguerre quadrature and, for cases of $a/b \geqslant 0.9$, two million points (zeros and weight factors) are needed to obtain convergent results.

When specifying the points along the quarter-circular generating arc of the fluid sphere (with a constant value of ϕ) where the boundary conditions are to be exactly satisfied, the first point that should be chosen is $\theta = \pi/2$, since this point defines the projected area of the droplet normal to the direction of motion and controls the gap between the droplet and the pore wall. In addition, the point $\theta = 0$ is also important. However, an examination of the system of linear algebraic equations in Eq. (16) shows that the matrix equation becomes singular if these points are used. To overcome this difficulty, these points are replaced by closely adjacent points, i.e., $\theta = \delta$ and $\pi/2 - \delta$ (Leichtberg et al., 1976). Additional points along the boundary are selected to divide the quarter-circular arc of the droplet into equal segments. The optimum value of δ in this work is found to be 0.01°, with which the numerical results of the hydrodynamic drag force acting on the particle converge satisfactorily.

The collocation solutions for the hydrodynamic drag force exerted on a fluid sphere translating along the axis of a circular cylindrical pore for various values of a/b and η^* are presented in Table 1 and Figs. 2 and 3. The drag force F_0 acting on an identical droplet in an unbounded fluid, given by Eq. (1) (with $\mathbf{F}_0 = F_0\mathbf{e}_z$), is used to normalize the boundary-corrected values. Evidently, $F/F_0 = 1$ as $a/b = 0$ for any given value of η^*. The accuracy and convergence behavior of the collocation/truncation technique depends principally upon the ratio a/b. All of the results obtained under this numerical scheme converge to at least the significant figures as shown in the table. For the difficult case of $a/b = 0.995$, the number of collocation points $N = 56$ is sufficiently large to achieve this convergence.

Through some approximate approaches in which the real external boundary of the flow in the infinitely long tube is replaced by a part of the lateral surface of the tube completed by two perpendicular cross sections situated at a finite distance from the particle, Hyman and Skalak (1972) and Coutanceau and Thizon (1981) obtained numerical solutions for the normalized hydrodynamic drag force acting on a fluid sphere moving along the axis of a circular tube. These solutions, which are available up to $a/b = 0.8$, are also presented in Table 1 for comparison. It can be seen that our collocation results agree very well with these numerical solutions. For the special case of a rigid sphere (with $\eta^* \to \infty$), our results also agree quite well with the previous solutions obtained by a method of reflection (Happel and Brenner, 1983) and by a similar boundary collocation method available up to $a/b = 0.7$ (Leichtberg et al., 1976).

Table 1
Collocation results for the normalized drag force F/F_0 experienced by a spherical droplet translating along the axis of a circular cylindrical pore at various values of a/b and $\eta*$

a/b	F/F_0							
	$\eta^* = 0$		$\eta^* = 1$		$\eta^* = 10$		$\eta^* \to \infty$	
0.1	1.16319	(1.164)	1.21114	(1.211)	1.25341	(1.253)	1.26321	(1.263)
0.2	1.38994	(1.391)	1.52091	(1.520)	1.64822	(1.648)	1.67948	(1.680)
0.25	1.53977	[1.5398]	1.73147	[1.7315]	1.92886		1.97908	[1.9796]
0.3	1.72510	(1.725)	1.99514	(1.996)	2.29156	(2.291)	2.37009	(2.370)
0.4	2.26263	(2.264)	2.76467	(2.765)	3.40436	(3.404)	3.59137	(3.592)
0.5	3.22243	(3.222)	4.11972	(4.123)	5.49200	(5.493)	5.94737	(5.949)
		[3.223]		[4.120]				[5.950]
0.6	5.20429	(5.205)	6.80703	(6.809)	9.88657	(9.891)	11.0919	(11.10)
0.7	10.2577	(10.26)	13.2196	(13.22)	20.9143	(20.93)	24.6759	(24.70)
0.75	16.1519	[16.2]	20.2758	[20.3]	33.3467		40.7267	[40.7]
0.8	28.5678	(28.59)	34.4183	(34.48)	58.4536	(58.64)	74.669	(74.97)
0.9	173.333		182.944		314.42		469.18	
0.95	1038.9		995.4		1590		2807	
0.975	6079		5478		7.86E3		1.63E4	
0.99	6.10E4		5.24E4		6.53E4		1.59E5	
0.995	3.3E5		2.8E5		3.2E5		8.0E5	

The values in parentheses obtained by Hyman and Skalak (1972) and in brackets obtained by Coutanceau and Thizon (1981) are listed for comparison.

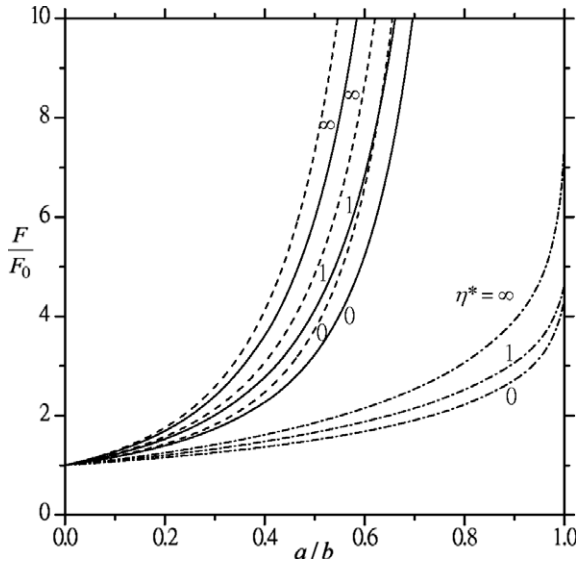

Fig. 2. Plots of the normalized drag force F/F_0 acting on a spherical droplet translating along the axis of a circular cylindrical pore versus the ratio a/b with η^* as a parameter (solid curves). The dashed and dotted-dashed curves are plotted for the corresponding translation of an identical droplet situated at the center of a spherical cavity and situated midway between two parallel plane walls, respectively, for comparison.

As expected, the results in Table 1 and Figs. 2 and 3 illustrate that the hydrodynamic drag force acting on the droplet is a monotonic increasing function of a/b, and will become infinite in the limit $a/b = 1$, for any given value of η^*. For cases that the radii of the droplet and pore are not too close (say, $a/b < 0.9$), the normalized wall-corrected drag force exerted on the droplet increases monotonically with an increase in η^*, keeping a/b unchanged. Interestingly, when the value of a/b is very close to unity (say, greater than about 0.9), F/F_0 first decreases with an increase in η^* from $\eta^* = 0$, reaches a minimum at some finite value of η^*, and then increases with an increase in η^* to the limit $\eta^* \to \infty$.

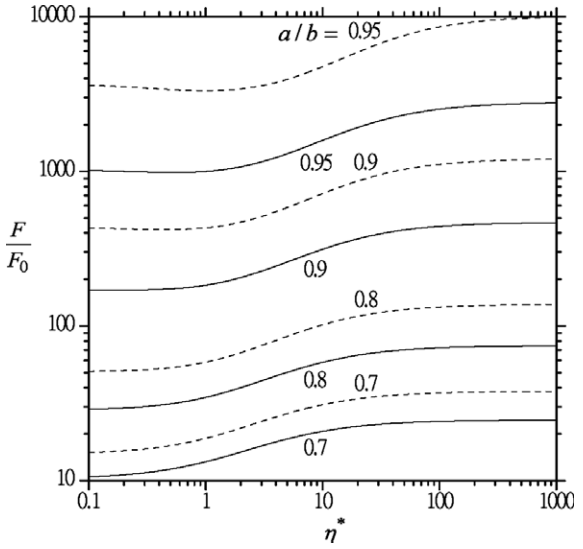

Fig. 3. Plots of the normalized drag force F/F_0 acting on a spherical droplet translating along the axis of a circular cylindrical pore versus its relative viscosity η^* with a/b as a parameter (solid curves). The dashed curves are plotted for the translation of an identical droplet situated at the center of a spherical cavity for comparison.

For the instantaneous translational motion of a spherical fluid droplet of radius a situated at the center of a spherical cavity of radius b, the normalized drag force exerted on the droplet by the surrounding fluid was analytically obtained as (Happel and Brenner, 1983)

$$\frac{F}{F_0} = \left(1 - \frac{\eta_{-3}}{\eta_2}\lambda^5\right)\left(1 - \frac{9\eta_2}{4\eta_3}\lambda + \frac{15\eta^*}{2\eta_3}\lambda^3 - \frac{9\eta_{-2}}{4\eta_3}\lambda^5 + \frac{\eta_{-3}}{\eta_3}\lambda^6\right)^{-1}, \tag{18}$$

where $\eta_i = 3\eta^* + i$ and $\lambda = a/b$. On the other hand, the steady translation of a fluid sphere parallel to two plane walls at an arbitrary position between them has been examined by using the boundary collocation technique and numerical solutions for the hydrodynamic drag force acting on the droplet were obtained as functions of η^* and the relative distances from the droplet center to the two plane walls (Keh and Chen, 2001). This drag force for the case that the droplet is situated midway between the two walls separated by a distance $2b$ and the drag result of Eq. (18) for the case of the droplet in a spherical cavity are also plotted in Figs. 2 and/or 3 as a comparison basis for the pore shape effect. It can be seen that, for given values of the parameters η^* and a/b, the droplet in a circular cylindrical pore acquires a lower hydrodynamic drag force than in a spherical cavity but a higher drag force than in a slit pore. This outcome is expected since a spherical cavity does not have an open fluid space to relax the momentum buildup when the droplet is applied an external force, and this momentum buildup can be relaxed in one and two principal directions for a circular cylindrical pore and a slit pore, respectively. Analogous to the case in a cylindrical pore, F/F_0 for the motion of a droplet located at the center of a spherical cavity is also an increasing function of η^* in general; when the value of a/b is close to unity (say, greater than about 0.9), this normalized drag force first decreases with an increase in η^* from $\eta^* = 0$, reaches a minimum at some finite value of η^*, and then increases with increasing η^* to the limit $\eta^* \to \infty$.

4. Formulation for the motion of a slip solid sphere along the axis of a slip cylindrical pore

The steady creeping motion caused by a solid spherical particle of radius a translating with a velocity $\mathbf{U} = U\mathbf{e}_z$ in a quiescent incompressible and Newtonian fluid along the axis of a long circular cylindrical pore of radius b, as shown in Fig. 1 again, is considered in this section. The fluid is allowed to slip at both the particle surface and the pore wall. Since the particle and pore are of different materials, they may have unequal slip coefficients at the surfaces. The objective is to determine the correction to Eq. (2) for the motion of the particle due to the presence of the pore wall.

The governing equation, the boundary condition at infinity, and the sufficiently general solution for the fluid flow are still given by Eqs. (4a), (9) and (10)–(12). Now, the boundary conditions for the fluid velocity at the particle surface and pore wall become (Basset, 1961; Happel and Brenner, 1983)

$$r = a: \quad v_\rho = \frac{1}{\beta}\tau_{r\theta}\cos\theta, \tag{19a}$$

$$v_z = U - \frac{1}{\beta}\tau_{r\theta}\sin\theta; \tag{19b}$$

$$\rho = b: \quad v_\rho = 0, \tag{20a}$$

$$v_z = -\frac{1}{\beta_w}\tau_{\rho z}, \tag{20b}$$

where $\tau_{r\theta}$ and $\tau_{\rho z}$ are the viscous shear stresses for the fluid flow in the relevant coordinates, and $1/\beta$ and $1/\beta_w$ are the frictional slip coefficients about the surfaces of the particle and pore wall, respectively. Substituting the stream function Ψ given by Eqs. (10)–(12) into the boundary condition (20) and applying the Fourier cosine transform on the variable z result in a solution for the functions $X(\omega)$ and $Y(\omega)$ in terms of the coefficients B_n and D_n. After the substitution of this solution back into Eqs. (10)–(12) and utilization of Eq. (5a) and the integral representations of the modified Bessel functions, the fluid velocity components can still be expressed in the form of Eq. (15), in which the functions $\gamma_{in}^{(j)}(r,\theta)$ for i and j equal to 1 or 2 are also defined by Eqs. (A.3) and (A.4) but now dependent on the wall slip coefficient $1/\beta_w$.

The only boundary conditions that remain to be satisfied are those on the particle surface. Substituting Eq. (15) into Eq. (19), one obtains

$$\sum_{n=2}^{\infty}\left\{B_n\left[\gamma_{1n}^{(1)}(a,\theta) - \frac{\eta}{\beta}\gamma_{1n}^{*}(a,\theta)\cos\theta\right] + D_n\left[\gamma_{2n}^{(1)}(a,\theta) - \frac{\eta}{\beta}\gamma_{2n}^{*}(a,\theta)\cos\theta\right]\right\} = 0, \tag{21a}$$

$$\sum_{n=2}^{\infty}\left\{B_n\left[\gamma_{1n}^{(2)}(a,\theta) + \frac{\eta}{\beta}\gamma_{1n}^{*}(a,\theta)\sin\theta\right] + D_n\left[\gamma_{2n}^{(2)}(a,\theta) + \frac{\eta}{\beta}\gamma_{2n}^{*}(a,\theta)\sin\theta\right]\right\} = U, \tag{21b}$$

where the functions $\gamma_{in}^{*}(r,\theta)$ for $i$and j equal to 1 or 2 are also dependent on the wall slip coefficient $1/\beta_w$ and have been defined by Eq. (A.12).

Eq. (21) can also be satisfied by utilizing the boundary collocation technique presented in Section 2 for the solution about a migrating droplet. At the particle surface, Eq. (21) is applied at N discrete points (values of θ between 0 and $\pi/2$) and the infinite series in Eqs. (15) and (21) are truncated after N terms. This generates a set of $2N$ linear algebraic equations for the $2N$ unknown constants B_n and D_n. The fluid velocity field is completely obtained once these coefficients are solved for a sufficiently large number of N. Again, the hydrodynamic drag force $\mathbf{F} = F\mathbf{e}_z$ acting on the spherical particle can be determined from Eq. (17).

5. Solutions for the motion of a slip solid sphere along the axis of a slip cylindrical pore

In Section 3, collocation solutions for the migration of a fluid sphere along the axis of a long circular cylindrical pore have been presented and were found to be in good agreement with the available solutions in the literature. This section will examine the solutions for the corresponding motion of a slip solid sphere using the same boundary collocation method. Now, the system of linear algebraic equations to be solved for the coefficients B_n and D_n is constructed from Eq. (21).

The collocation solutions of the hydrodynamic drag force acting on a slip spherical particle translating along the axis of a slip cylindrical pore for different values of the parameters $\beta a/\eta$, $\beta_w a/\eta$, and a/b are presented in Table 2 and Figs. 4 and 5. Here, the drag force F_0 exerted on an identical particle in an unbounded fluid given by Eq. (2) (with $\mathbf{F}_0 = F_0\mathbf{e}_z$) is used to normalize the boundary-corrected values. Obviously, $F/F_0 = 1$ as $a/b = 0$ for any specified values of $\beta a/\eta$ and $\beta_w a/\eta$. All of the results obtained under the collocation scheme converge satisfactorily to at least the significant figures shown in the table. For the special cases of translation of a no-slip sphere (with $\beta a/\eta \to \infty$) and of a perfectly slip sphere (with $\beta a/\eta = 0$) along the axis of a no-slip cylindrical pore (with $\beta_w a/\eta \to \infty$), our numerical results are exactly the same as those presented in Table 1 for

Table 2
Collocation results for the normalized drag force F/F_0 experienced by a spherical particle translating along the axis of a circular cylindrical pore at various values of a/b, β_w, and $\beta a/\eta$

	a/b	F/F_0					
		$\beta a/\eta = 0$	$\beta a/\eta = 0.1$	$\beta a/\eta = 1$	$\beta a/\eta = 10$	$\beta a/\eta = 30$	$\beta a/\eta \to \infty$
$\beta_w = 0$	0.2	1.28429	1.28987	1.32880	1.43188	1.46244	1.48301
	0.4	1.79341	1.81140	1.94294	2.35041	2.49145	2.59273
	0.6	2.94404	2.99316	3.37349	4.85185	5.50927	6.04615
	0.8	7.30773	7.48394	8.94210	16.8690	22.3431	28.5019
	0.9	19.1777	19.7199	24.3799	56.5988	89.2703	146.07
	0.95	52.0427	53.6351	67.6121	180.53	333.95	784.9
	0.975	143.951	148.540	189.289	550.98	1151.2	4323
	0.99	560.96	579.3	743.5	2300	5.312E3	4.17E4
	0.995	1578.6	1631	2098	6638	1.597E4	2.3E5
$\beta_w = \beta$	0.2	1.28429	1.29971	1.39014	1.58609	1.64185	1.67948
	0.4	1.79341	1.83131	2.10471	2.99068	3.33141	3.59137
	0.6	2.94404	3.04256	3.81055	7.25645	9.20702	11.0919
	0.8	7.30773	7.68212	10.7322	29.4427	46.9213	74.669
	0.9	19.1777	20.4029	30.5543	104.116	200.181	469.18
	0.95	52.0427	55.7891	87.076	335.57	737.0	2807
	0.975	143.951	155.004	247.69	1022.0	2444	1.63E4
	0.99	560.96	605.9	983.3	4243	1.079E4	1.59E5
	0.995	1578.6	1707	2786	1.220E4	3.17E4	8.0E5
$\beta_w \to \infty$	0.2	1.38994	1.39769	1.45243	1.60234	1.64821	1.67948
	0.4	2.26263	2.28871	2.48508	3.15199	3.40365	3.59137
	0.6	5.20429	5.27071	5.82728	8.47578	9.86146	11.0919
	0.8	28.5678	28.6504	29.9541	44.2658	57.3319	74.669
	0.9	173.333	172.287	168.989	218.18	296.47	469.18
	0.95	1038.9	1027.5	968.95	1068.5	1416.6	2807
	0.975	6079	5998	5538	5392	6631	1.63E4
	0.99	6.10E4	6.01E4	5.47E4	4.82E4	5.30E4	1.59E5
	0.995	3.3E5	3.3E5	3.0E5	2.5E5	2.6E5	8.0E5

the cases of $\eta^* \to \infty$ and $\eta^* = 0$, respectively, as they should be. However, the wall effect on the motion of a slip sphere with a finite value of $\beta a/\eta$ is different from that of a liquid droplet with a value of η^* equal to $\beta a/3\eta$, although the unbounded fluid flow field induced by the translation of a slip solid sphere is equivalent to the external flow field caused by an isolated translating fluid droplet under this condition.

As expected, the results in Table 2 and Figs. 4 and 5 illustrate that the normalized drag force exerted on the particle is a monotonic increasing function of a/b, and will become infinite in the limit $a/b = 1$, for any given values of $\beta a/\eta$ and $\beta_w a/\eta$. The normalized drag force in general increases with an increase in $\beta a/\eta$ and $\beta_w a/\eta$ (or with a decrease in the slip coefficients β^{-1} and β_w^{-1}), keeping the other parameters unchanged. When the cylindrical pore is hardly slip (with a large value of $\beta_w a/\eta$) and the value of a/b is close to unity (say, greater than about 0.9), however, F/F_0 first decreases with an increase in $\beta a/\eta$ from $\beta a/\eta = 0$, reaches a minimum at some finite value of $\beta a/\eta$, and then increases with increasing $\beta a/\eta$ to the limit $\beta a/\eta \to \infty$; some examples can be seen in Fig. 5b and Table 2.

For the quasisteady translational motion of a slip spherical particle of radius a situated at the center of a slip spherical cavity of radius b, the normalized drag force exerted on the particle by the fluid was analytically obtained as (Keh and Chang, 1998)

$$\frac{F}{F_0} = \frac{f_3}{f_2}(f_2 g_3 - f_{-3} g_{-2} \lambda^5)\left(f_3 g_3 - \frac{9}{4} f_2 g_2 \lambda + \frac{5}{2}\lambda^3 - \frac{9}{4} f_{-2} g_{-2} \lambda^5 + f_{-3} g_{-3} \lambda^6\right)^{-1}, \tag{22}$$

where $f_i = 1 + i\eta/\beta a$, $g_i = 1 + i\eta/\beta_w b$, and $\lambda = a/b$. This drag force is also plotted in Figs. 4b and 5 as a comparison. Under most conditions, the particle in a circular cylindrical pore acquires a lower hydrodynamic drag than in a spherical pore. This trend, however, can be reversed for the case of highly slippery particles and pore

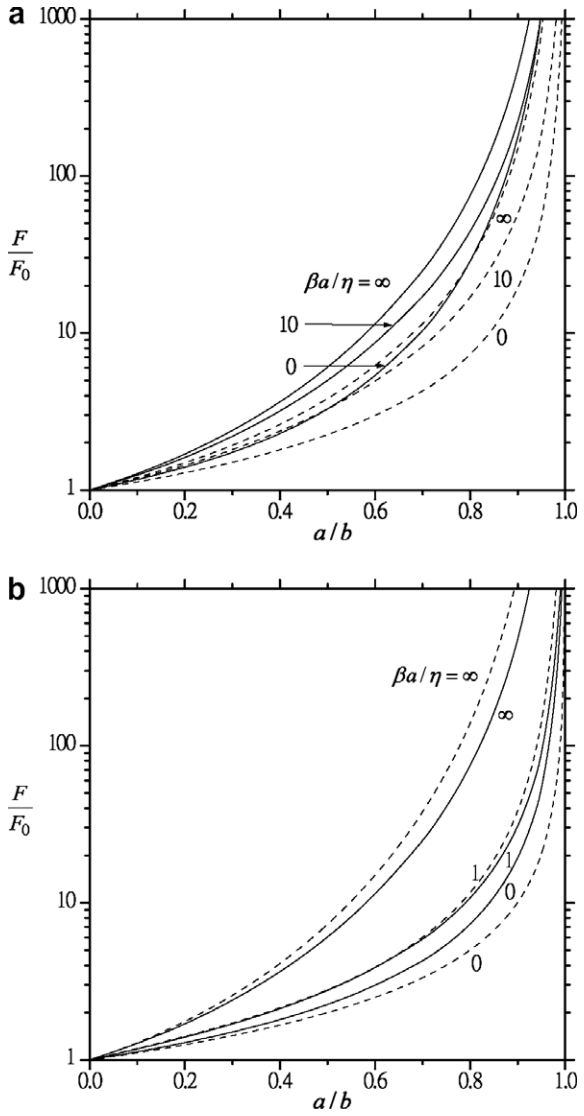

Fig. 4. Plots of the normalized drag force F/F_0 acting on a slip solid sphere translating along the axis of a circular cylindrical pore versus the ratio a/b with $\beta a/\eta$ as a parameter: (a) the solid and dashed curves represent the cases of $\beta_w \to \infty$ and $\beta_w = 0$, respectively and (b) the solid curves represent the case of $\beta_w = \beta$, while the dashed curves are plotted for the translation of an identical particle situated at the center of a spherical cavity for comparison.

walls (with small values of $\beta a/\eta$ and $\beta_w a/\eta$, say, less than about unity), as illustrated by curve intersections for each specified value of a/b in Fig. 5c–e. The smaller the value of $\beta_w a/\eta$ ($\beta a/\eta$) is, the greater value of $\beta a/\eta$ ($\beta_w a/\eta$) the curve intersections will take place at. For the case of $\beta_w a/\eta = 0$ and $a/b \leqslant 0.5$, as indicated by Fig. 5e, the fluid always exerts a smaller drag force on the particle in a spherical pore than in a cylindrical pore for any fixed value of $\beta a/\eta$. This outcome indicates that the slippage of the pore wall is more influential than that of the particle surface. Similar to the case in a cylindrical pore, when the value of a/b is close to unity (say, greater than about 0.9), F/F_0 for the motion of a slip sphere located at the center of a hardly slip spherical cavity also first decreases with an increase in $\beta a/\eta$ from $\beta a/\eta = 0$, reaches a minimum at some finite value of $\beta a/\eta$, and then increases with an increase in $\beta a/\eta$ to the limit $\beta a/\eta \to \infty$, as shown by two curves in Fig. 5b; otherwise, this normalized drag force is a monotonic increasing function of $\beta a/\eta$.

On the other hand, the steady translation of a slip solid sphere parallel to two no-slip plane walls at an arbitrary position between them has been examined by using the boundary collocation method and numerical

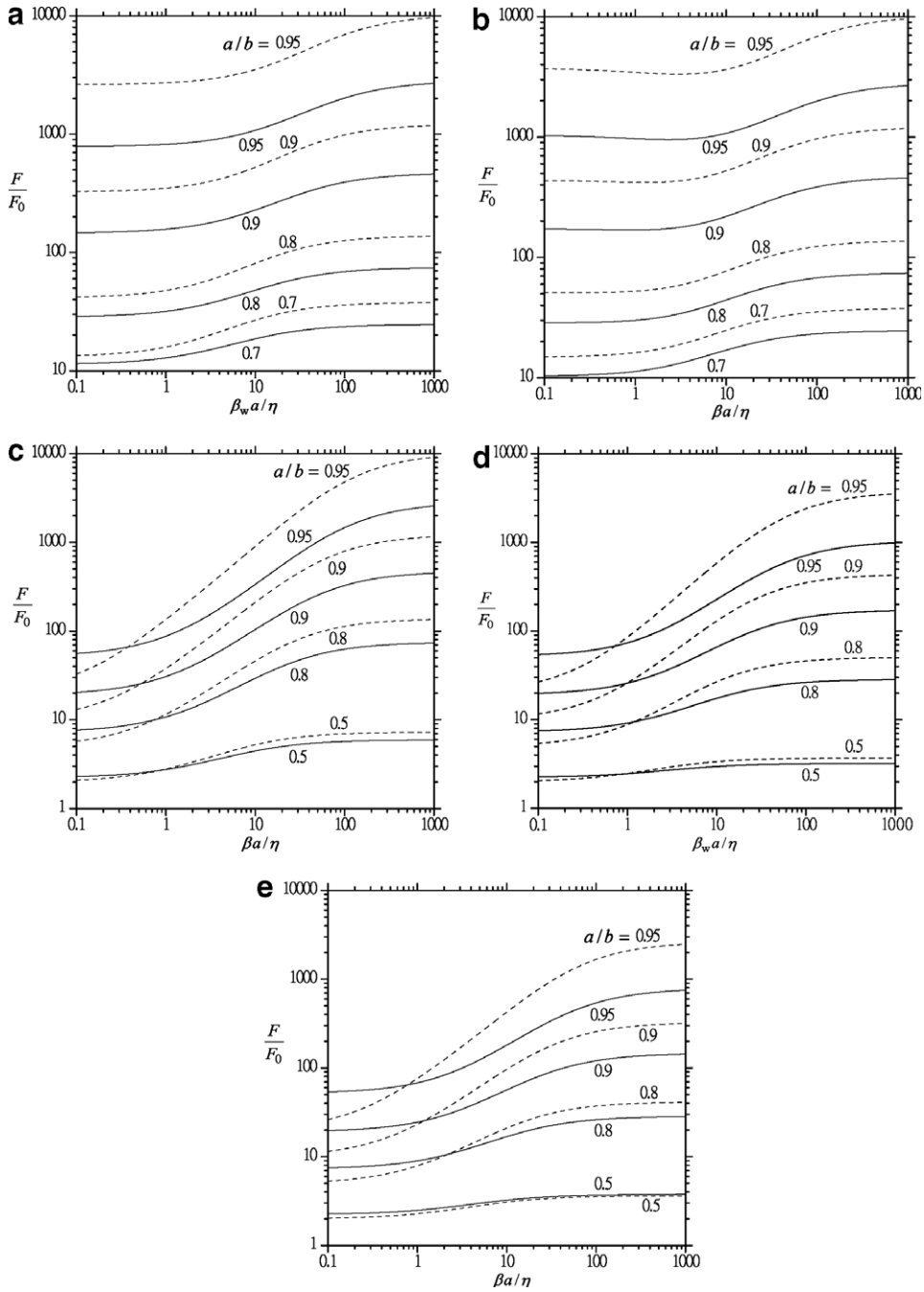

Fig. 5. Plots of the normalized drag force F/F_0 acting on a slip solid sphere translating along the axis of a circular cylindrical pore (solid curves) versus the slip parameter $\beta a/\eta$ or $\beta_w\, a/\eta$ with a/b as a parameter: (a) $\beta \to \infty$; (b) $\beta_w \to \infty$; (c) $\beta_w = \beta$; (d) $\beta = 0$; (e) $\beta_w = 0$. The dashed curves are plotted for the translation of an identical particle situated at the center of a spherical cavity for comparison.

solutions for the hydrodynamic drag force acting on the particle were obtained as functions of the slip parameter $\beta a/\eta$ and the relative distances from the particle center to the two plane walls (Chen and Keh, 2003). Analogous to the case of a fluid droplet discussed in Section 3, the drag force acquired by the parallel motion of a slip solid particle when placed midway between the two walls is much smaller than that for the translation of the particle along the axis of a circular cylindrical pore.

6. Concluding remarks

In this work the slow translational motions of a spherical fluid or solid particle in a viscous fluid along the axis of a circular cylindrical pore are studied theoretically, where the fluid may slip at the particle surface and pore wall. A semianalytical method with the boundary collocation technique has been used to solve the Stokes equations for the fluid flow field. The results for the hydrodynamic drag force exerted on the particle indicate that the solution procedure converges rapidly and accurate solutions can be obtained for various values of the particle's relative viscosity or slip coefficient, the wall slip parameter, and the relative separation distance between the particle and the confining boundary. It has been found that the wall-corrected drag force for each case increases monotonically with an increase in the ratio of particle-to-pore radii, and equals infinity in the limit. For a given ratio of particle-to-pore radii, the drag force acting on the particle normalized by the value in the absence of the pore in general is an increasing function of the internal-to-external viscosity ratio or a decreasing function of the dimensionless slip coefficients. When the pore wall is hardly slip and the value of the ratio of particle-to-pore radii is close to unity, however, the normalized drag force may not be a monotonic function of the particle's relative viscosity or slip coefficient.

Some comparisons for the pore shape effects on the axial translation of a slip sphere have been made in Sections 3 and 5. Under most conditions, the particle in a circular cylindrical pore acquires a lower hydrodynamic drag force than in a spherical cavity but a higher drag force than in a slit pore. This trend, however, can be reversed for the case of highly slippery particles and pore walls.

In Tables 1 and 2 as well as Figs. 2–5, we presented only the results for resistance problems, defined as those in which the drag force F exerted by the surrounding fluid on the particle translating near the confining boundary is to be determined for a specified particle velocity U[equal to $-(F_0/6\pi\eta a)(3\eta^* + 3)/(3\eta^* + 2)$ or $-(F_0/6\pi\eta a)(\beta a + 3\eta)/(\beta a + 2\eta)$]. In a mobility problem, on the other hand, the external force F [equal to $6\pi\eta a U_0(3\eta^* + 2)/(3\eta^* + 3)$ or $6\pi\eta a U_0(\beta a + 2\eta)/(\beta a + 3\eta)$] imposed on the particle is specified and the boundary-corrected particle velocity U is to be determined. For the creeping motion of a spherical particle along the axis of a cylindrical pore considered in this work, the ratio U/U_0 for a mobility problem equals the ratio $(F/F_0)^{-1}$ for its corresponding resistance problem. Thus, our results can also be applied to physical problems in which the applied force on the particle is the prescribed quantity and the particle must move accordingly.

Throughout Sections 2 and 3, we assume a spherical shape for the fluid droplet in the cylindrical pore. This is correct for the creeping motion as the radius ratio a/b is small. When the value of a/b is relatively close to unity, however, it is not necessarily the case for all capillary numbers, even quite small. In earlier studies, a solution that calculates the droplet deformation requires a numerical approach such as a finite difference method (Reinelt, 1987), finite element method (Westborg and Hassager, 1989), or boundary integral equation technique (Martinez and Udell, 1990; Pozrikidis, 1992). On the other hand, it would be beneficial to compare previous and our calculations to numerical results that can be obtained using an available commercial code such as FLUENT of FEMLAB for a sequence of decreasing capillary numbers. Of course, a comparison of our results in Table 1 for the case of $a/b > 0.8$, where no solution in this range is available in the literature, can also be provided by such a commercial code.

Acknowledgement

Part of this research was supported by the National Science Council of the Republic of China.

Appendix A. Definitions of some functions in Sections 2 and 4

The functions $\alpha_{\text{in}}^{(j)}$ and $\gamma_{\text{in}}^{(j)}$ for i and j equal to 1 or 2 in Eqs. (14)–(16) and (21) are defined by

$$\alpha_{\text{in}}^{(1)}(r,\theta) = -r^{n+2i-4}[(n+1)G_{n+1}^{-1/2}(\cos\theta)\csc\theta - (2n+2i-3)G_n^{-1/2}(\cos\theta)\cot\theta], \tag{A.1}$$

$$\alpha_{\text{in}}^{(2)}(r,\theta) = -r^{n+2i-4}[(2n+2i-3)G_n^{-1/2}(\cos\theta) + P_n(\cos\theta)]; \tag{A.2}$$

$$\gamma_{\text{in}}^{(1)}(r,\theta)=\int_0^\infty\left[S_i^{(1)}(\omega)I_0(\omega r\sin\theta)r\sin\theta+S_i^{(2)}(\omega)I_1(\omega r\sin\theta)\right]\omega\sin(\omega r\cos\theta)\,\mathrm{d}\omega$$
$$-r^{-n+2i-3}\left[(n+1)G_{n+1}^{-1/2}(\cos\theta)\csc\theta-2(i-1)G_n^{-1/2}(\cos\theta)\cot\theta\right], \tag{A.3}$$

$$\gamma_{\text{in}}^{(2)}(r,\theta)=\int_0^\infty\{S_i^{(1)}(\omega)[2I_0(\omega r\sin\theta)+I_1(\omega r\sin\theta)\omega r\sin\theta]+\omega S_i^{(2)}(\omega)I_0(\omega r\sin\theta)\}$$
$$\times\cos(\omega r\cos\theta)\,\mathrm{d}\omega-r^{-n+2i-3}[P_n(\cos\theta)+2(i-1)G_n^{-1/2}(\cos\theta)]. \tag{A.4}$$

In Eqs. (A.3) and (A.4),

$$S_i^{(1)}(\omega)=\frac{A_{\text{in}}^{(1)}(\omega)\left[I_0(b\omega)+\frac{2\eta}{\beta_w}\omega I_1(b\omega)\right]-A_{\text{in}}^{(2)}(\omega)I_1(b\omega)}{b\omega I_0^2(b\omega)-2I_0(b\omega)I_1(b\omega)-\left(b+\frac{2\eta}{\beta_w}\right)\omega I_1^2(b\omega)}, \tag{A.5}$$

$$S_i^{(2)}(\omega)=\frac{A_{\text{in}}^{(1)}(\omega)-b\omega I_0(b\omega)S_i^{(1)}(\omega)}{\omega I_1(b\omega)}, \tag{A.6}$$

where

$$A_{1n}^{(1)}(\omega)=-(-1)^{n/2}\frac{2\omega^n}{\pi n!}K_1(b\omega), \tag{A.7}$$

$$A_{2n}^{(1)}(\omega)=(-1)^{n/2}\frac{2\omega^{n-2}}{\pi n!}[(n-2)(n-3)K_1(b\omega)-(2n-3)b\omega K_0(b\omega)], \tag{A.8}$$

$$A_{1n}^{(2)}(\omega)=(-1)^{n/2}\frac{2\omega^n}{\pi n!}\left[K_0(b\omega)-\frac{2\eta}{\beta_w}\omega K_1(b\omega)\right], \tag{A.9}$$

$$A_{2n}^{(2)}(\omega)=(-1)^{n/2}\frac{2\omega^{n-2}}{\pi n!}\left\{\left[(2n-3)b\omega+\frac{2\eta}{\beta_w}\omega(n^2-3n+3)\right]K_1(b\omega)\right.$$
$$\left.-\left[n(n-1)+\frac{2\eta}{\beta_w}b\omega^2(2n-3)\right]K_0(b\omega)\right\}, \tag{A.10}$$

and I_n and K_n are the modified Bessel functions of the first and second kinds, respectively, of order n. Note that $\beta_w\to\infty$ for all functions appearing in Section 2.

The functions α_{in}^* and γ_{in}^* for i equal to 1 or 2 in Eqs. (16d) and (21) are defined by

$$\alpha_{\text{in}}^*(r,\theta)=-r^{n+2i-5}[(n+1)(n+2i-5)G_{n+1}^{-1/2}(\cos\theta)\cot\theta$$
$$-(n+2i-5)(2n+2i-3)G_n^{-1/2}(\cos\theta)\csc\theta$$
$$+(5-2i+n\cot^2\theta)P_n(\cos\theta)\sin\theta-nP_{n-1}(\cos\theta)\cot\theta], \tag{A.11}$$

$$\gamma_{\text{in}}^*(r,\theta)=-\cos\theta\sin\theta[C_{\text{in}}^*(r,\theta)+D_{\text{in}}^*(r,\theta)]-(\cos^2\theta-\sin^2\theta)[C_{\text{in}}^{**}(r,\theta)+D_{\text{in}}^{**}(r,\theta)], \tag{A.12}$$

where

$$C_{1n}^*(r,\theta)=-2r^{-(n+2)}\left[(n+1)(n+\csc^2\theta)G_{n+1}^{-1/2}(\cos\theta)-(3n+2)P_n(\cos\theta)\cos\theta\right.$$
$$\left.+nP_{n-1}(\cos\theta)\right], \tag{A.13}$$

$$C_{2n}^*(r,\theta)=2r^{-n}\left[2(2n-1+\cot^2\theta)G_n^{-1/2}(\cos\theta)\cos\theta-(n+1)(n-1+\cot^2\theta)G_{n+1}^{-1/2}(\cos\theta)\right.$$
$$\left.-(n+2-4\sin^2\theta)P_{n-1}(\cos\theta)+3nP_n(\cos\theta)\cos\theta\right], \tag{A.14}$$

$$C_{1n}^{**}(r,\theta) = -r^{-(n+2)}\Big\{n\cot\theta\Big[(n+1)G_{n+1}^{-1/2}(\cos\theta) + P_{n-1}(\cos\theta)\Big]. + [(3n+2)\sin\theta - n\csc\theta]P_n(\cos\theta)\Big\}, \tag{A.15}$$

$$C_{2n}^{**}(r,\theta) = -r^{-n}\Big\{2[2(n-1)\sin\theta - (n-2)\csc\theta]G_n^{-1/2}(\cos\theta). + (n^2-n-2)G_{n+1}^{-1/2}(\cos\theta)\cot\theta + (n-4\sin^2\theta)P_{n-1}(\cos\theta)\cot\theta + n(3\sin\theta - \csc\theta)P_n(\cos\theta)\Big\}; \tag{A.16}$$

$$D_{\mathrm{in}}^{*}(r,\theta) = -2\int_0^\infty \Big\{S_i^{(1)}[3I_0(\omega r\sin\theta) + 2\omega r\sin\theta I_1(\omega r\sin\theta)] + S_i^{(2)}[2\omega I_0(\omega r\sin\theta) - I_1(\omega r\sin\theta)/r\sin\theta]\Big\}\omega\sin(\omega r\cos\theta)\,\mathrm{d}\omega, \tag{A.17}$$

$$D_{\mathrm{in}}^{**}(r,\theta) = -2\int_0^\infty \Big\{S_i^{(1)}[I_1(\omega r\sin\theta) + \omega r\sin\theta I_0(\omega r\sin\theta)]. + S_i^{(2)}\omega I_1(\omega r\sin\theta)\Big\}\omega\cos(\omega r\cos\theta)\,\mathrm{d}\omega. \tag{A.18}$$

References

Bart, E., 1968. The slow unsteady settling of a fluid sphere toward a flat fluid interface. Chem. Eng. Sci. 23, 193–210.

Basset, A.B., 1961. In: A Treatise on Hydrodynamics, vol. 2. Dover, New York.

Beavers, G.S., Joseph, D.D., 1967. Boundary conditions at a naturally permeable wall. J. Fluid Mech. 30, 197–207.

Brenner, H., 1971. Pressure drop due to the motion of neutrally buoyant particles in duct flows. II. Spherical droplets and bubbles. Ind. Eng. Chem., Fund. 10, 537–542.

Chang, Y.C., Keh, H.J., 2006. Slow motion of a slip spherical particle perpendicular to two plane walls. J. Fluids Struct. 22, 647–661.

Chen, P.Y., Keh, H.J., 2003. Slow motion of a slip spherical particle parallel to one or two plane walls. J. Chin. Instit. Chem. Eng. 34, 123–133.

Chen, S.H., Keh, H.J., 1995. Axisymmetric motion of two spherical particles with slip surfaces. J. Colloid Interf. Sci. 171, 63–72.

Coutanceau, M., Thizon, P., 1981. Wall effect on the bubble behaviour in highly viscous liquids. J. Fluid Mech. 107, 339–373.

Davis, M.H., 1972. Collisions of small cloud droplets: Gas kinetic effects. J. Atmos. Sci. 29, 911–915.

Gogte, S., Vorobieff, P., Truesdell, R., Mammoli, A., van Swol, F., Shah, P., Brinker, C.J., 2005. Effective slip on textured superhydrophobic surfaces. Phys. Fluids 17, 051701.

Haberman, W.L., Sayre, R.M., 1958. Motion of rigid and fluid spheres in stationary and moving liquids inside cylindrical tubes. Davis Taylor Model Basin Report 1143, Washington, DC.

Hadamard, J.S., 1911. Mouvement permanent lent d'une sphere liquid et visqueuse dans un liquide visqueux. Comptes Rendus Hebdomadaires des Seances de V Acad des Sci (Paris) 152, 1735–1738.

Happel, J., Brenner, H., 1983. Low Reynolds Number Hydrodynamics. Nijhoff, Dordrecht, The Netherlands.

Hetsroni, G., Haber, S., Wacholder, E., 1970. The flow fields in and around a droplet moving axially within a tube. J. Fluid Mech. 41, 689–705.

Hutchins, D.K., Harper, M.H., Felder, R.L., 1995. Slip correction measurements for solid spherical particles by modulated dynamic light scattering. Aerosol Sci. Technol. 22, 202–218.

Hyman, W.A., Skalak, R., 1972. Viscous flow of a suspension of liquid drops in a cylindrical tube. Appl. Sci. Res. 26, 27–52.

Jones, I.P., 1973. Low Reynolds number flow past a porous spherical shell. Proc. Cambridge Philos. Soc. 73, 231–238.

Keh, H.J., Chang, J.H., 1998. Boundary effects on the creeping-flow and thermophoretic motions of an aerosol particle in a spherical cavity. Chem. Eng. Sci. 53, 2365–2377.

Keh, H.J., Chen, P.Y., 2001. Slow motion of a droplet between two parallel plane walls. Chem. Eng. Sci. 56, 6863–6871.

Kennard, E.H., 1938. Kinetic Theory of Gases. McGraw-Hill, New York.

Leichtberg, S., Pfeffer, R., Weinbaum, S., 1976. Stokes flow past finite coaxial clusters of spheres in a circular cylinder. Int. J. Multiphase Flow 3, 147–169.

Lu, S.Y., Lee, C.T., 2001. Boundary effects on creeping motion of an aerosol particle in a non-concentric pore. Chem. Eng. Sci. 56, 5207–5216.

Martinez, M.J., Udell, K.S., 1990. Axisymmetric creeping motion of drops through circular tubes. J. Fluid Mech. 210, 565–591.

Nir, A., 1976. Linear shear flow past a porous particle. Appl. Sci. Res. 32, 313–325.

O'Brien, V., 1968. Form factors for deformed spheroids in Stokes flow. A.I.Ch.E. J. 14, 870–875.

Pozrikidis, C., 1992. The buoyancy-driven motion of a train of viscous drops within a cylindrical tube. J. Fluid Mech. 237, 627–648.
Reed, L.D., Morrison, F.A., 1974. Particle interactions in viscous flow at small values of Knudsen number. J. Aerosol Sci. 5, 175–189.
Reinelt, D.A., 1987. The rate at which a long bubble rises in a vertical tube. J. Fluid Mech. 175, 557–565.
Rushton, E., Davies, G.A., 1973. The slow unsteady settling of two fluid spheres along their line of centres. Appl. Sci. Res. 28, 37–61.
Rybczynski, W., 1911. Uber die fortschreitende bewegung einer flussigen kugel in einem zahenmedium. Bull. Acad. Sci. Cracovie Ser. A 1, 40–46.
Saffman, P.G., 1971. On the boundary condition at the surface of a porous medium. Studies Appl. Math. 50, 93–101.
Shapira, M., Haber, S., 1988. Low Reynolds number motion of a droplet between two parallel plates. Int. J. Multiphase Flow 14, 483–506.
Sharipov, F., Kalempa, D., 2003. Velocity slip and temperature jump coefficients for gaseous mixtures. I. Viscous slip coefficient. Phys. Fluids 15, 1800–1806.
Stokes, G.G., 1851. On the effect of the internal friction of fluid on pendulums. Trans. Cambridge Philos. Soc. 9, 8–106.
Talbot, L., Cheng, R.K., Schefer, R.W., Willis, D.R., 1980. Thermophoresis of particles in heated boundary layer. J. Fluid Mech. 101, 737–758.
Tretheway, D.C., Meinhart, C.D., 2002. Apparent fluid slip at hydrophobic microchannel walls. Phys. Fluids 14, L9–L12.
Wacholder, E., Weihs, D., 1972. Slow motion of a fluid sphere in the vicinity of another sphere or a plane boundary. Chem. Eng. Sci. 27, 1817–1828.
Westborg, H., Hassager, O., 1989. Creeping motion of long bubbles and drops in capillary tubes. J. Coll. Interf. Sci. 133, 135–147.